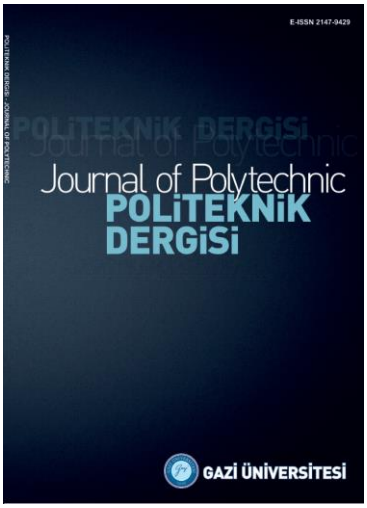

POLİTEKNİK DERGİSİ

JOURNAL of POLYTECHNIC

ISSN: 1302-0900 (PRINT), ISSN: 2147-9429 (ONLINE)
URL: http://dergipark.gov.tr/politeknik

Comparative process parameter optimization for wire arc additive manufacturing (WAAM) of E120C-GH4 metal cored and ER120S-G solid wire

E120C-GH4 metal özlü ve ER120S-G masif telin tel ark eklemeli imalatı için karşılaştırmalı proses parametre optimizasyonu

***Yazar(lar) (Author(s))**: Mustafa HARMAN[1], Cemil ÇETİNKAYA[2], Oğuzhan YILMAZ[3], Nevzat BOL[4]*

ORCID[1]: 0000-0001-6045-0570

ORCID[2]: 0000-0002-0298-1143

ORCID[3]: 0000-0002-2641-2324

ORCID[4]: 0000-0001-6700-7707

To cite to this article: Harman M., Çetinkaya C., Yılmaz O. ve Bol N. "Comparative Process Parameter Optimization For Wire Arc Additive Manufacturing (WAAM) of E120C-GH4 Metal Cored and ER120S-G Solid Wire", ***Journal of Polytechnic***, 27(5): 2013-2028, (2024).

Bu makaleye şu şekilde atıfta bulunabilirsiniz: Harman M., Çetinkaya C., Yılmaz O. ve Bol N. "Comparative Process Parameter Optimization For Wire Arc Additive Manufacturing (WAAM) of E120C-GH4 Metal Cored and ER120S-G Solid Wire", ***Politeknik Dergisi***, 27(5): 2013-2028, (2024).

Erişim linki (To link to this article): http://dergipark.gov.tr/politeknik/archive

DOI: 10.2339/politeknik.1478172

Comparative Process Parameter Optimization For Wire Arc Additive Manufacturing (WAAM) of E120C-GH4 Metal Cored and ER120S-G Solid Wire

Highlights

- *The WAAM process parameters were optimized for two wires at the same three different heat inputs.*
- *Metal-cored high-strength and solid wire were compared at different wire feeding speeds and heat inputs.*
- *The Taguchi optimization method was applied in Minitab to compute multiple regression analyses.*
- *Macro-section examination and macro-hardness measurement processes were performed on 36 samples.*
- *Metal-cored wires superiority at production time and deposition rate were proven by experiments.*

Graphical Abstract

Real experiments were conducted with metal-cored wire and solid wire of the same composition at different heat inputs and torch advance speeds in wire-fed arc melting manufacturing (WAAM), macro section and hardness examinations, and Taguchi optimization in terms of production time and metal deposition rate.

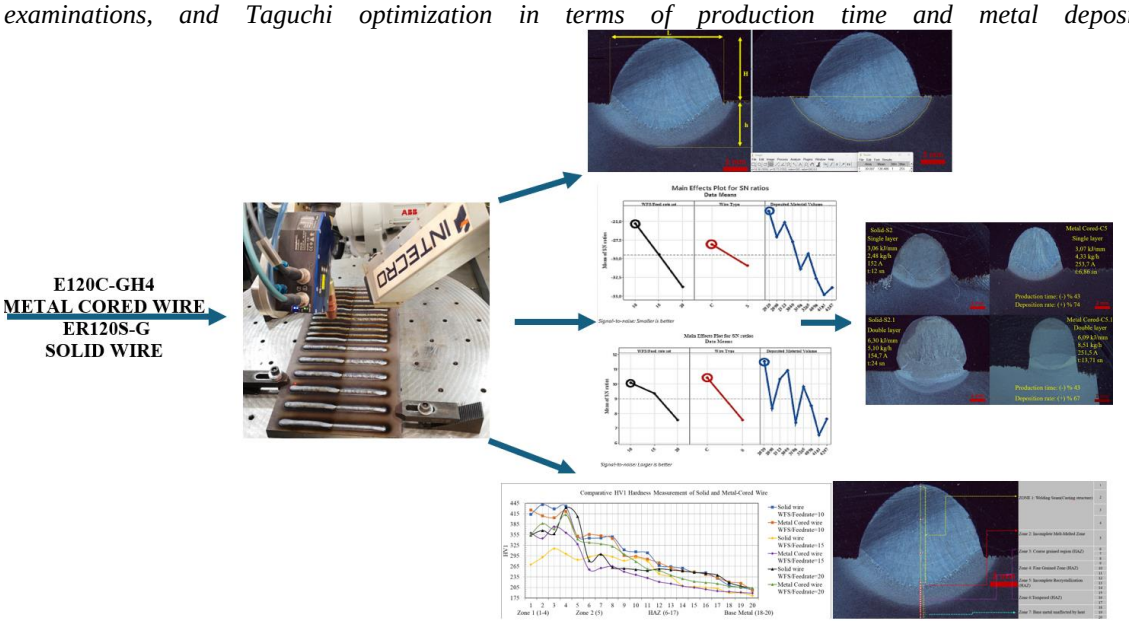

Figure. Experimental results of wires optimized by Minitab (Taguchi) and produced by the WAAM.

Aim

To reach the optimum result with optimization and experimental methods by comparing the armor steel solid and metal-cored wires used in WAAM in terms of metal deposition rate and deposition time at the same metal deposition volume and heat inputs.

Design & Methodology

Welding seams were produced using the wire arc additive manufacturing method (WAAM). Macro sectioning, hardness measurement, analysis, and geometric measurements were performed with the Minitab and ImageJ programs.

Originality

It is the first study to date in the WAAM method using high-strength armor steel metal-cored wire, which reduces production time by 43% and increases the deposition rate by 74% at the lowest heat input.

Findings

C5 was the most ideal sample according to the Minitab Taguchi method and experimental conclusions clearly.

Conclusion

Cored wire reduced the production time by fifty percent compared to solid wire, and cored wire had a higher deposition rate (1,74 times that of solid wire), faster melting conditions, and higher hardness values compared to solid wire.

Declaration of Ethical Standards

The author(s) of this article announce that the materials and methods used in this investigation do not need ethical committee consent and/or lawful special consent.

Comparative Process Parameter Optimization For Wire Arc Additive Manufacturing (WAAM) of E120C-GH4 Metal Cored and ER120S-G Solid Wire

Araştırma Makalesi / Research Article

Mustafa HARMAN[1,2*], Cemil ÇETİNKAYA[3], Oğuzhan YILMAZ[4], Nevzat BOL[5]

[1*]Fen Bilimleri Enstitüsü, Metalurji ve Malzeme Müh.Bölümü Mezunu, Gazi Üniversitesi, Ankara, Türkiye
[2*]Rektörlük, Yapı İşleri ve Teknik Daire Başkanlığı, Çankırı Karatekin Üniversitesi, Çankırı, Türkiye
[3]Teknoloji Fakültesi, Metalurji ve Malzeme Müh.Bölümü, Gazi Üniversitesi, Ankara, Türkiye
[4]Mühendislik Mimarlık Fakültesi, Makine Müh. Bölümü, Gazi Üniversitesi, Ankara, Türkiye
[5]Intecro Robotik A.Ş, Ankara, Türkiye

(Geliş/Received : 03.05.2024 ; Kabul/Accepted : 21.07.2024 ; Erken Görünüm/Early View: 08.08.2024)

ABSTRACT

The wire arc additive manufacturing (WAAM) method is a metal additive manufacturing method that allows the production of large and medium-complexity parts layer by layer by considering the part-specific CAD model. Process parameters were optimized to achieve minimum heat input, less production time, a higher metal deposition rate, and bead geometry with a thin, high, and adequate weld bead depth of influence. E120C-GH4 metal-cored seamless high-strength wire with a diameter of 1.2 mm and an ER120S-G solid wire of the same diameter were used at different wire feeding speeds employing different heat input levels (namely low, medium, and high). Single- and double-layer 18 beads were deposited with each of these wires. Samples were prepared for macro section examination and macro hardness measurement processes. Samples with similar deposition volumes were compared in terms of bead geometry, micro hardness, penetration depth, deposition time, and the metal deposition rate at the same heat input. With the aid of the Taguchi method, the samples were subjected to multiple regression analyses. So, the analyses and real experiments allowed for comparative experimental studies. Considering the cost and time, the result shows that metal-cored wire will be much preferable for the WAAM industry because metal-cored wire has 43% less production time and a 74% higher metal deposition rate than solid wire.

Keywords: Metal cored wire, Taguchi method, Armor steel, WAAM, macro section.

E120C-GH4 Metal Özlü ve ER120S-G Masif Telin Tel Ark Eklemeli İmalatı İçin Karşılaştırmalı Proses Parametre Optimizasyonu

ÖZ

Tel ark eklemeli imalat (WAAM) yöntemi, parçaya özel CAD modeli dikkate alınarak büyük ve orta karmaşıklıktaki parçaların katman katman üretilmesine olanak sağlayan bir metal eklemeli imalat yöntemidir. Proses parametreleri, minimum ısı girdisi, daha az üretim süresi, daha yüksek metal biriktirme oranı, daha ince ve yüksek kaynak dikiş geometrisi ile yeterli kaynak nüfuziyet derinliğine sahip dikiş elde etmek üzere optimize edildi. 1,2 mm çapındaki E120C-GH4 metal özlü dikişsiz yüksek mukavemetli tel ile yine aynı çapta ER120S-G masif tel farklı tel besleme hızları ve farklı ısı girdisi seviyelerinde (yani düşük, orta ve yüksek) kullanıldı. Bu tellerin her biri ile tek ve çift katmanlı olmak üzere 18'er adet dikiş biriktirildi. Numuneler Makro kesit incelemesi ve makro sertlik ölçümü işlemleri için hazırlandı. Eşit biriktirme hacmine sahip numuneler aynı ısı girdisinde dikiş geometrisi, mikro sertlik, penetrasyon derinliği, biriktirme süresi ve metal biriktirme hızı açısından karşılaştırıldı. Numuneler Taguchi yöntemi yardımıyla çoklu regresyon analizine tabi tutuldu. Böylece, analiz çalışmaları sayesinde gerçek deneysel sonuçların karşılaştırılması yapılabildi. Sonuçlar, maliyet ve zaman bakımından, metal özlü telin WAAM endüstrisi için daha çok tercih edileceğini göstermiştir çünkü metal özlü tel, masif tele göre % 43 daha az üretim süresine ve % 74 daha yüksek metal biriktirme oranına sahiptir.

Anahtar Kelimeler: Metal özlü tel, Taguchi metodu, zırh çeliği, WAAM, makro kesit.

1. INTRODUCTION

Apart from conventional production methods (forging, casting, etc.) and known machining methods (milling, turning, grinding, etc.), in the additive manufacturing method, parts are manufactured by welding them layer by layer [1]. As seen in Figure 1. Additive manufacturing (AM), known as 3D production, is now increasingly used in every field and has brought a different perspective to all kinds of designs, especially advanced engineering materials [2]. AM, particularly WAAM, which is also known as the arc-directed energy deposition (Arc-DED) process, has been more attractive in terms of energy efficiency, low cost, and short production time compared to conventional machinin processes that allow

* *Corresponding Author*
e-mail : mustafa.harman@gazi.edu.tr

manufacturing from a solid model [1–3]. Different from other subtractive and AM processes, WAAM can maintain and enhance the mechanical properties of the base metal [4].

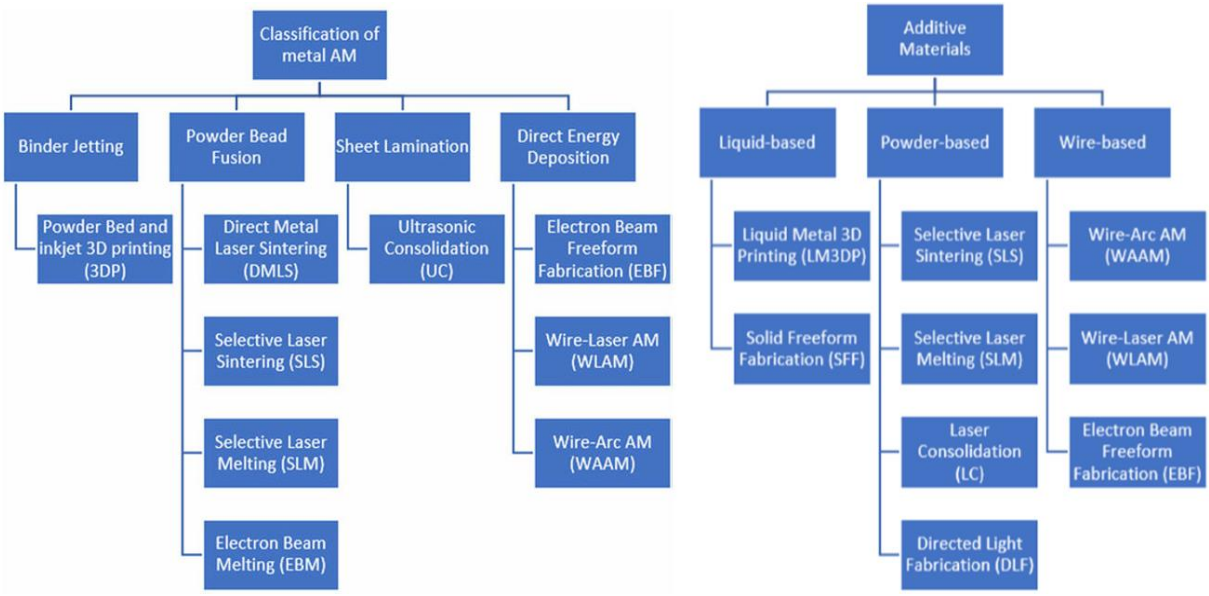

Figure 1. Classification of metal AM technologies and state of additive materials for 3D metal printing [9].

Gas-metal arc welding is based on the basic operating logic of WAAM. Parts are produced with multilayer deposition by controlling the basic variable parameters of the process, such as heat input, wire feeding speed, feed speed, torch angle, current, voltage, distance between torch (CTWD: contact tip to work distance) and base, torch position (push, pull, neutral), interlayer waiting time, maximum temperature between layers, preheating temperature, t8/5 (cooling time from 800 °C to 500 °C) is the cooling time, and tool path selection [5, 14]. Side-by-side and overlapping welding seams directly affect the surface waviness, dimensional accuracy, and mechanical technological properties [6, 7]. These produced parts are not suitable for use in their final form. Therefore, these parts are brought to the required surface dimensions by milling and grinding to obtain the final product. The more the need for post-processing operations can be reduced, the more the effectiveness of the WAAM process will increase [10].

In plasma-WAAM welding and tungsten inert gas welding, the movement of the additive material wire into the welding pool is provided by an external wire feeding unit, while in GMAW-WAAM there is an internal unit that sends the wire to the tip of the torch at a certain speed through rollers. Thanks to the melting speed of the wire, which varies according to the roughness (weld pool waviness) of the weld seam surface (height of weld pool volume), the continuous movement of the weld pool can be controlled more easily in WAAM. Selecting appropriate design variables and optimizing WAAM process parameters can prevent residual stresses and distortion in the material, as is known [11]. Studies conducted to date have shown that the gas metal arc welding (GMAW)-based WAAM technique reduces the production cost of large-sized components [12]. These components can consist of a variety of materials, including stainless steels, titanium alloys, low-alloy high-strength steels, aluminum alloys, and many more [15–19].

As seen in Figure 2. The WAAM process consists of a 1-power supply, 2-wire feeding unit, 3-torch, 4-hose package, 5-crash box, and robot flange [13].

Figure 2. WAAM process components [8]

Parameters affecting WAAM production: heat input, wire feeding speed, torch travel speed, torch angle, current, voltage, CTWD, torch position (push, pull, neutral), interlayer waiting time, maximum temperature between layers, preheating temperature, t8/5 (cooling time from 800°C to 500°C) [2, 14].CTWD was applied for both wires as CTWD: 12 mm, 10 times the wire

diameter in short arc mode, as described in DIN 1910 Part 1 in Figure 3. During production, each nozzle was measured and checked with a caliper during cleaning.

Kind of arc	Current contact tube-to-work distance k [mm]
Short arc	About 10 x wire diameter
Long arc	About 8 – 12 x wire diameter
Spray-arc	About 12 – 16 x wire diameter

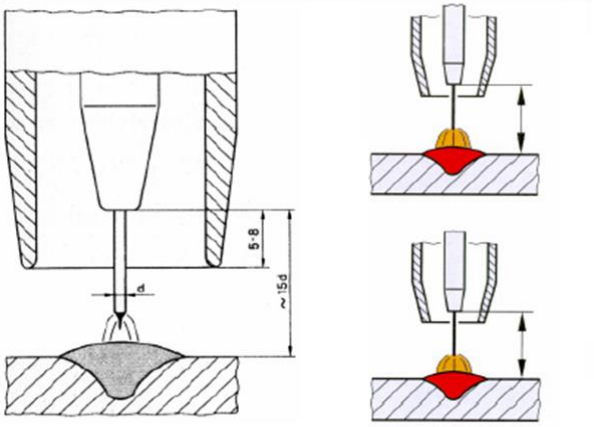

Figure 3. CTWD: contact tip to work distance according to DIN 1910 Part 1.

In the WAAM production method, the Total Materia (TM) material database provided the mechanical, electrical, physical, and technological properties of the material of the part to be produced with specific parameters that provided the same heat input [20]. Thermal conductivity (W/m·°C), thermal expansion (10^-6/°C), and thermal capacity (J/°C) of flux-cored wire, solid wire, and S355 substrate materials depending on temperature (especially between 800 °C and 500 °C) values were obtained from the TM material database. Process parameters that provided these features were programmed into the robot control unit and welding machine using the Taguchi optimization method [21–24]. As a result of production, these predetermined process parameters were verified by visual inspection, macrostructure examination, and hardness measurement with the WAAM procedure.

In the welded manufacturing of armor steels, there are some factors affecting t8/5 (cooling time from 800 °C to 500 °C) and the critical cooling rate [19, 25]. These factors are the maximum temperature of the austenite phase, the speed of reaching the austenite phase temperature, the waiting time at the austenite temperature, the time for the austenite phase to cool to 500 °C, the atmospheric environment (type of shielding gas) where the austenite temperature is reached, and finally the composition of the material [25]. For these factors, in the WAAM method, welding must be done quickly, and the heat input to the material must be kept at the lowest level thanks to the cold metal transfer (CMT) mechanism in the welding machine [26–29]. The CMT welding machine sends a signal that retracts the weld filler wire. It detects a short circuit, giving the weld pool time to cool before each drop is placed in the weld pool. Thanks to the CMT mechanism, the material's (high-strength steel wire) microstructure was less affected by austenite phase temperatures. And also, with the help of the CMT mechanism, the cooling time of high-strength steels from 800 °C to 500 °C was kept minimal, and so the material's strength was preserved. In the literature, armor steel parts were produced by using low-alloy, high-strength solid wire at the WAAM method [30].

However, today, it is possible to produce parts with less welding wire and in a shorter time with metal-cored wires with a similar composition to solid wire, only with a different production method [31, 32]. Additionally, metal-cored wires had higher dynamic toughness values than solid wires in the same composition [33, 34]. With a different structure from solid wires, the metal-cored wires presented developed features to produce high-strength steel parts [29–35]. Reducing the production waiting times and maintaining the hardness and strength of the main material were the developed features [36, 37]. In particular, the production precision of seamless metal-cored wires produced by using high-frequency welding was higher than that of other flux-cored wires [14–38]. The cost of metal-cored wire is slightly higher than that of solid wire in small amounts of production. However, in small-scale production, the production of solid wire from ingot is more expensive. In this case, it is more economical to fix the required chemical composition in metal-cored wire. Metal-cored wires do not need slag removal in each layer, as do flux-core wires. Different from metal-cored wires, FCW use is limited because it requires slag removal.

In previous studies, E110C-K4 metal-cored wire and ER100S-G solid wire were compared in terms of mechanical properties. It was observed that metal-cored wire exhibited a smoother penetration profile and gave higher values than solid wire in terms of mechanical properties. Since metal-cored wires allowed high current density, the deposition rate also increased in these wires [39, 40]. In the literature, previous research concentrated on the effect of different interlayer temperatures (150°C–350°C–600°C) on WAAM [5]. In this research, Zhai et al. obtained the highest tensile strength at 350°C, and they observed no significant change in the microstructure at interlayer temperatures of 150°C and 350°C. At 600 °C, although the loss of strength was not very significant, wall collapses occurred.

As a result, the temperature increment from 150°C to 350°C increased the metal deposition rate and also provided maximum tensile strength in the material. It was concluded that in the WAAM application of high-strength metal-cored wire, the lowest limit of the interlayer temperature was 150 °C, while the highest limit was 350 °C [5]. There hasn't been any study regarding the E120C-GH4 metal-cored seamless high-strength wire, which can provide the mechanical and technological properties expected from the material in WAAM [38].

Different from the literature, in this study, WAAM process parameters were optimized in terms of minimum

heat input, less production time, a higher metal deposition rate, and bead geometry for solid and metal-cored wires. Also, the study examined the effects of wire types on the deposition rate, deposition time at the same deposited material volume, and bead length. The researcher's findings indicated the relationship of wire feed speed (WFS) with a deposition rate (DR), weld bead depth of influence (h), bead width (L), and bead height (H) for both wires.

2. MATERIAL and METHOD

2.1. Material

In this study, 18 single-layer and 18 double-layer depositions were deposited from each wire using WAAM (wire arc additive method) using ER120S-G solid wire [41] and E120C-GH4 metal-cored wire [42]. The wires were of the same standard and similar composition, but the manufacturing method of the wires was different. The solid wire electrode used in this study was made from high-strength steel itself and was coated with copper to prevent oxidation and aid electrical conductivity [41]. Copper plating also helped to increase the life of the welding contact tip [41]. Metal-cored wire was obtained from Yuneka Metal Welding Fronius Böhler Company, and the metal-cored wire's production process consisted of nine stages [42, 43]. These stages were listed below in items.

1. Non-alloy strip material was fed in
2. Production of the tube from the strip using high-frequency welding
3. Cleaning the inside of the tube and heat treatment in a furnace
4. Production of the powder mixture
5. Filing of the tube using vibration
6. Pre-drawing and heat treatment of the filled tube
7. Drawing to the final dimension
8. Coating with copper
9. Coiling the wire for delivery to the customer

Table 1. shows the chemical compositions and mechanical properties of the wire's and substrate metal's materials. The values were guaranteed by the manufacturer in Table 1. S355JR was obtained from Fimak Optik Limited Company. The mechanical properties and chemical compositions of S355JR were in accordance with EN 10025-2. In WAAM deposition, the process parameters included a wire diameter of 1.2 mm, a shielding gas of % 82 Ar-+ CO2 %18, and an interpass temperature of 200 °C.

Table 1. The chemical compositions and mechanical properties of the wire's materials.

Chemical compositions (%)							Mechanical properties				
Material	C	Si	Mn	Cr	Ni	Mo	Material	Yield (MPa)	Tensile (MPa)	Elongation (%)	Fracture Energy (Joule) (KV)
E120C-GH4 Metal Cored Wire	0,06	0,7	1,9	0,5	2,1	0,4	E120C-GH4 Metal Cored Wire	≥ 890	≥ 940	≥ 17	≥ 70 (-50ºC)
ER120S-G Solid Wire	0,1	0,8	1,8	0,35	2,25	0,6	ER120S-G Solid Wire	≥ 890	≥ 940	≥ 15	≥ 47 (-60ºC)
S355JR	0,2	0,55	1,6	-	-	-	S355JR	355	470-630	20	-

2.2. Method

The experimental setup is shown in Figure 4.(a). In the study, two 400 x 200 x 20 mm S355JR base plates were prepared by cutting in a water jet. S235 plates were fixed to the positioner table in the Metalworm System seen in Figure 4.a.

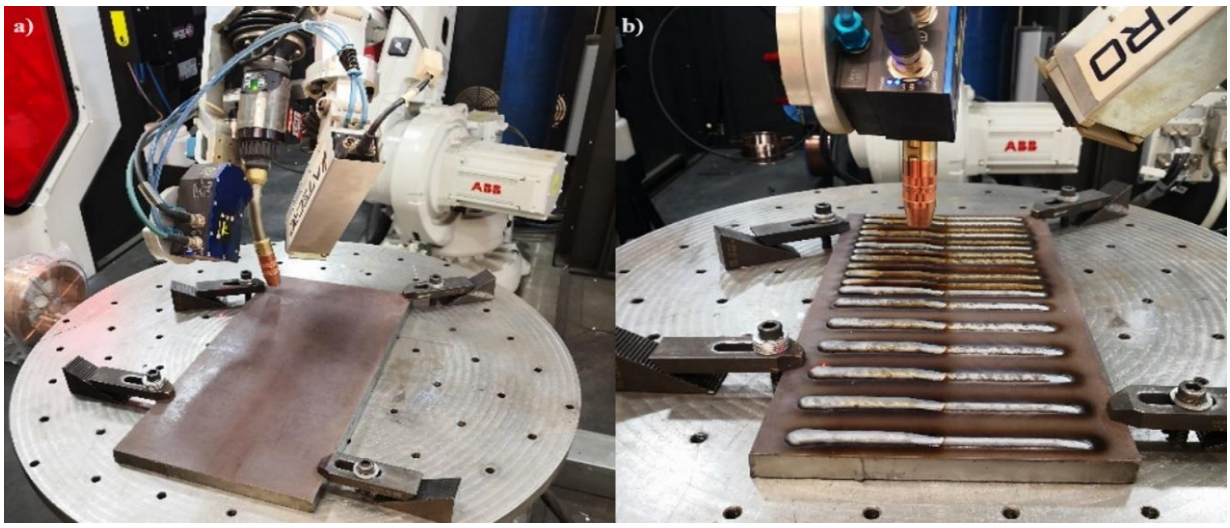

Figure 4. (a) Metalworm: 6-axis industrial robot, (b) deposited beads on the substrate.

The metalworm machine and each wire were used to produce welding beads in two layers with eighteen different parameters in the S355JR steel base, thanks to Intecro Robotics Company's contributions. The machine system consists of a 6-axis industrial robot arm, a two-axis positioner, and special sensor and camera equipment. The Fronius TPS500i CMT (Cold Metal Transfer) power source welding machine in the Metalworm gave the minimum heat input to preserve the mechanical properties of the base material [26–28, 44]. Before starting the study, the parameters given in Table 2 and Table 3 were determined according to the Taguchi L18 orthogonal index method. E120C-GH4 Metal Cored Wire and ER120S-G Solid wire wires were deposited on separate substrates as a 160-mm-long layer weld seam in an 82% Ar+/18% CO2 protective gas atmosphere at a gas flow rate of 20 L/min.

Then, when the interpass temperature dropped below 200 °C, a second layer of 80 mm-long seam was deposited. Images of the finished production are given in Figure 4.b. Deposition processes were carried out according to the parameters given in Table 2 and Table 3. The experimental procedure was planned for optimizing the main parameters of the process, which were composed of wire feed speed (WFS) and torch travel speed (TTS). 18 weld seams, single and double-layered, were deposited on the substrates, as shown in Figures 4.b and 5.(a). The production stages on the Metalworm machine were monitored and recorded with the in-bench optical camera and thermal cameras shown in Figure 5.(b). During production, control parameters and result parameters were also monitored on the digital control panel screen of the machine, as shown in Figure 5.(c).

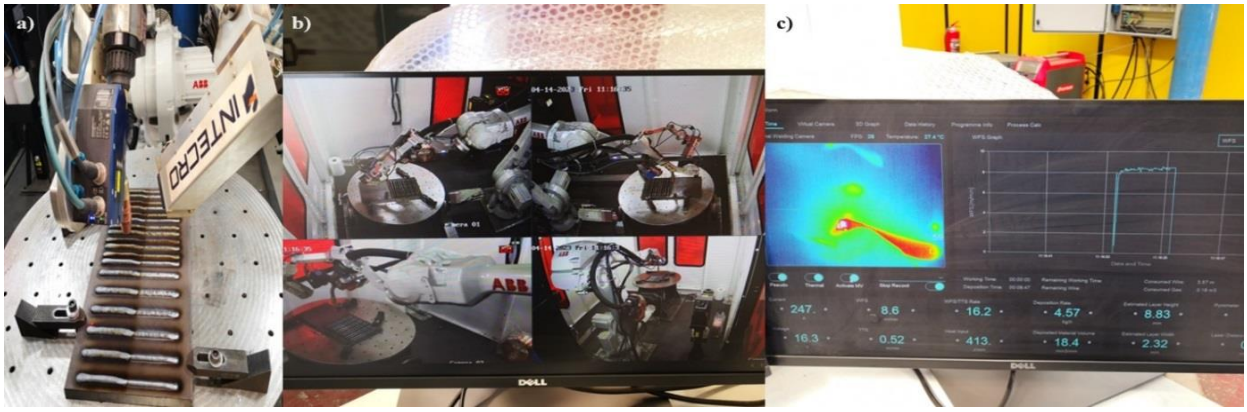

Figure 5. (a) Deposited beads, (b) Metalworm bench camera images (c) Metalworm digital control panel.

The layers of solid wire produced on the Metalworm machine are shown in Figure 6.(a), and the layers of metal-cored wire are seen in Figure 6.(b). Two finished substrates were cut on the water jet machine capable of angular cutting, as shown in Figure 7 (a). Then, the cut samples were removed for macrostructure examination.

Figure 6. (a) Layers of solid wire, (b) Layers of metal-cored wire

The cut samples and cutting paths are given in Figure 7. (b) To prevent the cut surfaces of the samples from being affected by heat, the weld beads were cut in the waterjet cutting machine [44]. Waterjet machine cutting parameters: cutting speed: 43.36 mm/min, and cutting nozzle diameter: 0.3 mm. During the production of solid wire and metal-cored wire, the parameters given in Table 2. and Table 3. (current, voltage, welding speed, etc.) were different for both wires. It was studied at the same heat input values. There was no splash that would affect the deposited material volume values. Solid wire test parameters were given in Table 2., and metal-cored wire test parameters were also given in Table 3. The main purpose of this study is to comparatively examine the macro properties and hardness values of the wires compared at the same heat input. Heat input (Q) is defined as the amount of heat per mm of the weld seam length during the welding of a pass or layer [45, 57]. The heat input is formulated as Q (kJ/mm) =η x I (ampere) x U (volt) x 60/1000 x TTS (mm/min.). The energy efficiency factor in the formula is symbolized by η, and TTS (torch travel speed) is the welding speed.

The energy efficiency factor ɳ varies according to welding methods and was taken as "0.8" in MAG (solid wire) welding and "0.9" in MAG (cored wire) welding [45]. Therefore, in the heat input formula given above, the potential effects of current and voltage values and welding speed values were already included in the applied optimization study.

Figure 7. (a) Waterjet cutting (b) Samples after cutting

Table 2. Solid wire test parameters

Heat input intensity	Wire Type and first layer numbers	Current (Amper)	Voltage (Volt)	WFS/TTS	WFS	Torch travel speed (TTS) (m/dk)	Wire feed speed (WFS) m/min	WFS/TTS	Welding Time (second)	Heat Input (kJ/cm)	Deposited Rate (kg/h)
LOW	S1	116,2	13,7	10	3	0,30	3,5	11,6	32,00	2,86	1,85
	S2	152,0	14,8	10	4	0,40	4,7	11,8	24,00	3,06	2,48
	S3	173,7	15,5	10	5	0,50	5,6	11,2	19,20	2,91	2,97
	S4	190,1	15,9	10	6	0,60	6,3	10,5	16,00	2,72	3,30
	S5	222	16,3	10	7	0,70	7,3	10,4	13,71	2,81	3,90
	S6	247,0	16,4	10	8	0,80	8,4	10,5	12,00	2,74	4,46
MEDIUM	S7	113,9	13,4	15	3	0,20	3,4	17,1	48,00	4,17	1,80
	S8	152,2	14,8	15	4	0,27	4,8	18,0	36,00	4,60	2,50
	S9	172,6	15,1	15	5	0,33	5,5	16,5	28,80	4,28	2,90
	S10	191,2	15,6	15	6	0,40	6,2	15,5	24,00	4,07	3,28
	S11	222,0	16,2	15	7	0,47	7,0	15,2	20,57	4,20	3,74
	S12	245,7	16,5	15	8	0,53	8,3	15,8	18,00	4,16	4,44
HIGH	S13	120,0	13,7	20	3	0,15	3,6	24,0	64,00	5,92	1,92
	S14	152,3	14,5	20	4	0,20	4,7	23,5	48,00	6,04	2,48
	S15	172,7	15,3	20	5	0,25	5,6	22,6	38,40	5,78	2,97
	S16	190,1	15,8	20	6	0,30	6,2	20,8	32,00	5,42	3,32
	S17	222,1	16,3	20	7	0,35	7,0	20,2	27,43	5,62	3,74
	S18	247,3	16,2	20	8	0,40	8,0	20,2	24,00	5,45	4,25

Table 3. Metal-cored wire test parameters

Wire Type and first layer numbers	Current (Amper)	Voltage (Volt)	WFS/TTS	WFS	Torch travel speed (TTS) (m/dk)	Wire feed speed (WFS) m/min	WFS/TTS	Welding Time (second)	Heat Input (kJ/cm)	Deposited Rate (kg/h)
C1	127,3	12,7	10	3	0,3	10,7	10,7	32,00	2,91	1,71
C2	160,1	13,75	10	4	0,4	10,9	10,9	24,00	3,00	2,30
C3	184,8	14,7	10	5	0,5	10,8	10,8	19,20	2,94	2,85
C4	220,2	15,4	10	6	0,6	11,5	11,5	16,00	3,05	3,69
C5	253,7	15,6	10	7	0,7	11,7	11,7	13,71	3,07	4,33
C6	272,8	15,7	10	8	0,8	11,2	11,2	12,00	2,90	4,78
C7	122,7	12,7	15	3	0,2	15,8	15,8	48,00	4,23	1,67
C8	157,8	13,6	15	4	0,3	16,2	16,2	36,00	4,38	2,28
C9	193,0	14,7	15	5	0,3	17,3	17,3	28,80	4,63	3,03
C10	224,8	15,3	15	6	0,4	18,0	18,0	24,00	4,70	3,81
C11	251,1	15,7	15	7	0,5	17,3	17,3	20,57	4,60	4,25
C12	270,2	15,8	15	8	0,5	17,2	17,2	18,00	4,37	4,82
C13	130,7	12,8	20	3	0,2	22,7	22,7	64,00	6,04	1,81
C14	161,9	13,6	20	4	0,2	22,6	22,6	48,00	6,01	2,39
C15	198,2	14,3	20	5	0,3	22,9	22,9	38,40	6,21	3,01
C16	219,9	15,0	20	6	0,3	22,4	22,4	32,00	5,96	3,59
C17	253,6	15,1	20	7	0,3	22,7	22,7	27,43	5,96	4,21
C18	272,4	15,2	20	8	0,4	22,1	22,1	24,00	5,66	4,65

The bakelite process in Figure 8. (a), automatic sanding, and automatic polishing in Figure 8 (b) were applied to the cut samples in the Gazi University Metallurgy Laboratory. The polished samples, 3 µm polycrystalline diamond suspension, and polishing felt can be seen in Figure 8.(c). Automatic sanding was carried out for 10 minutes at a speed of 300 rpm and under a load of 30 Newton's with coolant. The direction of rotation of the sample and the sanding table worked in the same direction. The automatic polishing process was applied in 10 minutes at a speed of 150 rpm and under a load of 25 Newton's. During the application, 9 µm and 3 µm polycrystalline diamond suspensions were used, respectively, and the samples were rotated in opposite directions with the polishing felt.

Figure 8. a) Bakelite process, b) Automatic sanding and polishing, c) Polished samples

After the polishing process, the samples were etched with a 2% Nital (2 ml HNO3, 98 ml ethyl alcohol) solution for 20–30 seconds. Macrostructure analyses of the etched samples were carried out in the Gazi University Faculty of Technology Metallurgical and Materials Engineering laboratories. Leica DM 4000M metal microscope is shown in Figure 9. (a) was used in this analysis.

Figure 9. a) Sample examination in metal microscope, b) Macro hardness measurement processes in Qness

The hardness measurements were carried out by the Qness Q30 M model hardness measuring device. The Vickers hardness measuring method is shown in Figure 9. (b) was used in these measurements. They were carried out under a load of 1 kg. One example macro-section view is given in Figure 10. As seen in Figure 11, the solid wire and metal-cored wire bead geometry macro-section images were processed with the ImageJ program. In Figure 11, H (mm) is weld bead height, h (mm) is weld bead depth of influence, and L (mm) is weld bead width. Taguchi, Regression analyses were performed in the Minitab software. The most effective parameters were determined by the Anova module in Minitab software. The program made polynomial regression analyses for two wires. The relationship between independent variables such as WFS/feed rate set, WFS, wire type and dependent variables such as DR, t, H, h was transformed into equations thanks to these analyses.

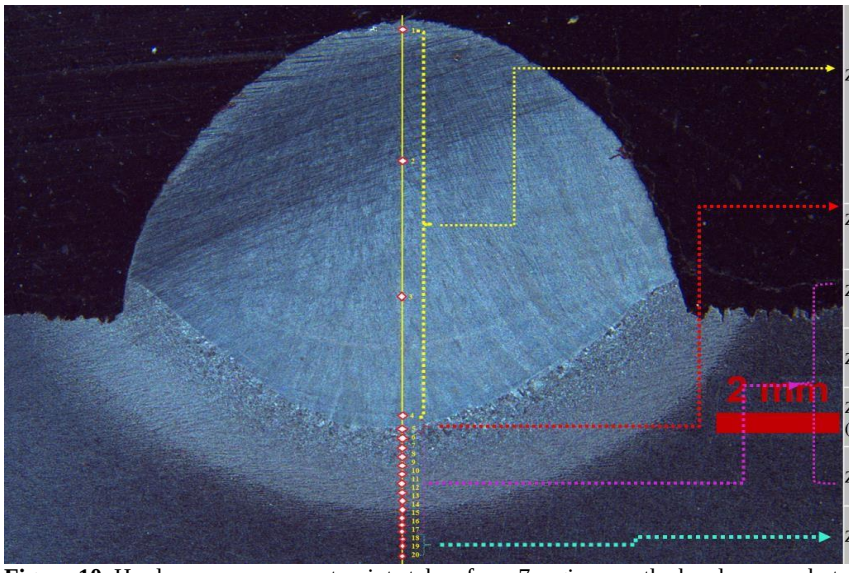

ZONE 1: Welding Seam(Casting structure)	1, 2, 3, 4
Zone 2: Incomplete Melt-Melted Zone	5
Zone 3: Coarse grained region (HAZ)	6, 7, 8
Zone 4: Fine Grained Zone (HAZ)	9, 10, 11
Zone 5: Incomplete Recrystallization (HAZ)	12, 13, 14
Zone 6:Tempered (HAZ)	15, 16, 17
Zone 7: Base metal unaffected by heat	18, 19, 20

Figure 10. Hardness measurement points taken from 7 regions on the bead macro photo.

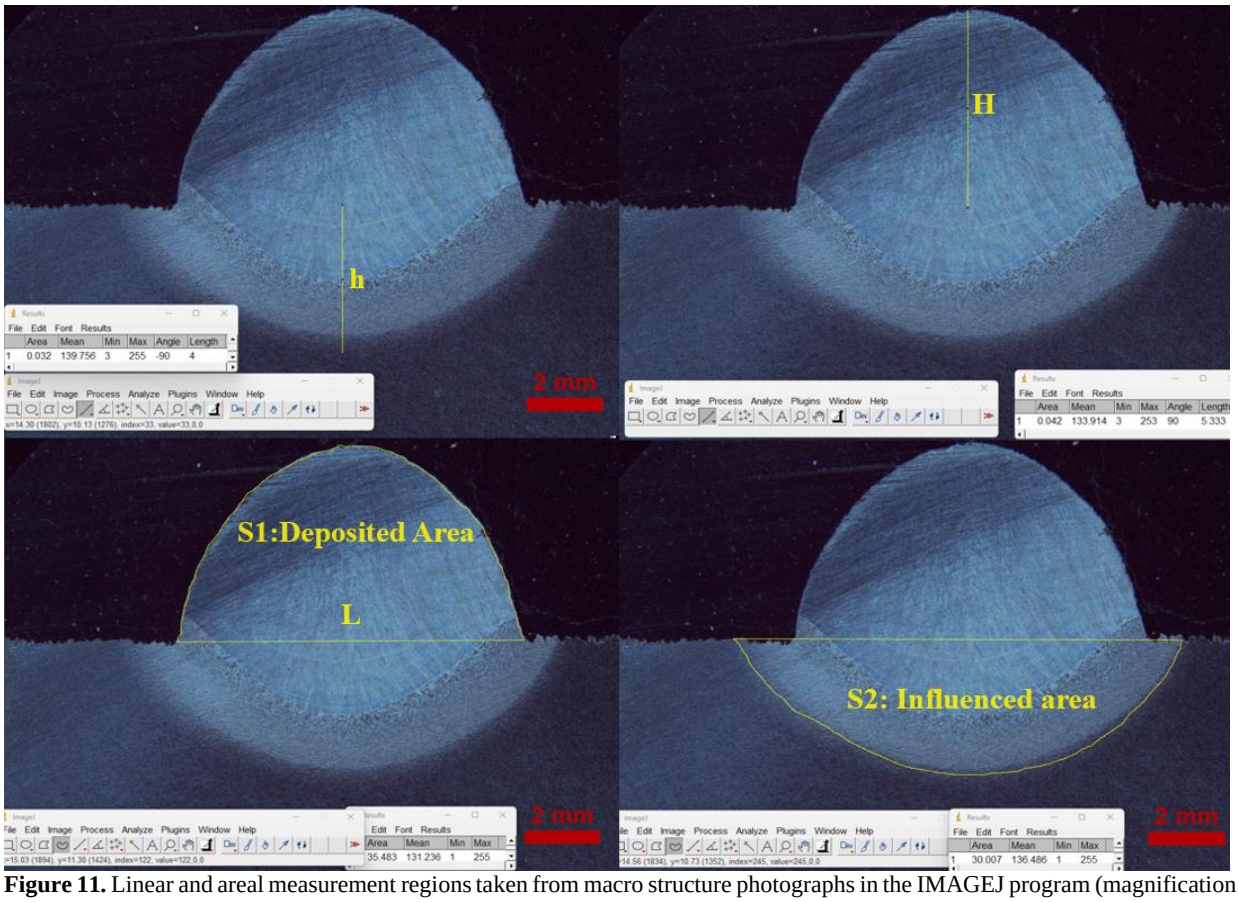

Figure 11. Linear and areal measurement regions taken from macro structure photographs in the IMAGEJ program (magnification rate: 10X)

3. EXPERIMENTAL RESULTS

3.1. Results of Optimization Studies in Minitab

According to the Taguchi L18 orthogonal array method, the predetermined parameters in Table 2 and Table 3 for both wires were used in the Minitab program. This program processed the results obtained by the Taguchi method and variance analyses for both real experiments, as shown in Table 5. In this table, sample value pairs were divided into three groups in terms of heat input intensity at the same deposited material volume: S1-C4; S2-C5; S3-C6; S7-C9; S8-C10; S9-C11; S13-C13; S14-C14; and S15-C15. Deposited material volume at 160 mm of bead length was used for comparing wires at the same heat

input intensity. Control parameters for the nine-piece weld beads of each wire are also given in Table 5. Different heat inputs were applied to the wires, and the deposition volumes were kept constant for comparison. Thus, the effect of different heat inputs on the results could be analyzed more accurately. According to the Taguchi analysis results, when the deposited material volume was kept constant throughout the total bead, the most ideal value pairs were computed. When considering the maximum deposition rate and minimum welding time, the most ideal value pairs were found by three groups: C6-S3; C11-S9; and C5-S2. Since a lack of fusion defect was observed at the double layer of the C6.1 and S3.1 macro sections, these samples were excluded from evaluation. Double-layer bead geometry was coded as C6.1 and S3.1. All other double-layer bead geometries were also examined by coding in this way. The observed defects are given in Figure 12.

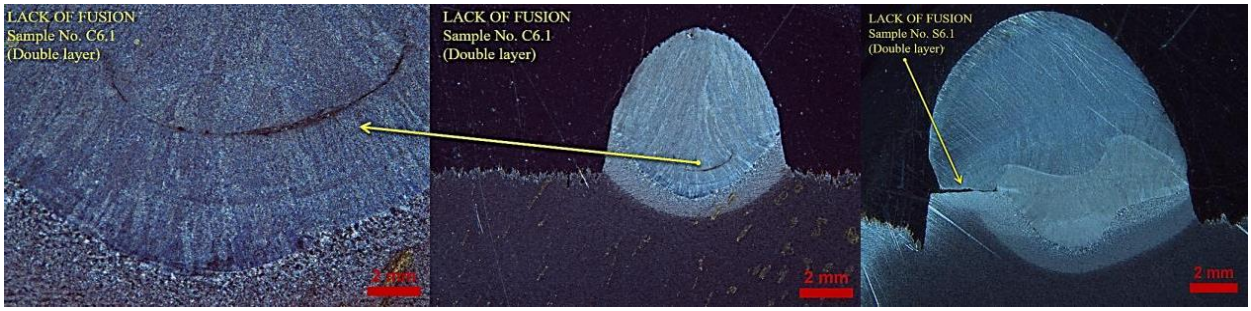

Figure 12. Lack of fusion defects at double layers of C6.1 and S3.1 macro sections

Minitab Program made polynomial regression analyses for two wires depending on real and predicted equations comparing results of bead geometry (BG), deposition rate (DR), weld bead height (H), heat input (HI), and weld time (t). The relationship between independent variables such as WFS/feed rate set, WFS, and wire type and dependent variables such as DR, t, H, h was transformed into equations thanks to these analyses. In terms of the lowest heat input, in this case, the C5-S2 experimental pair was the most ideal comparative sample group according to the Minitab Taguchi method signal-to-noise ratios. So, Figure 16.(b) and Table 4. show C5 as a most ideal sample according to the average S/N ratio for t (sec) DR (kg/h).

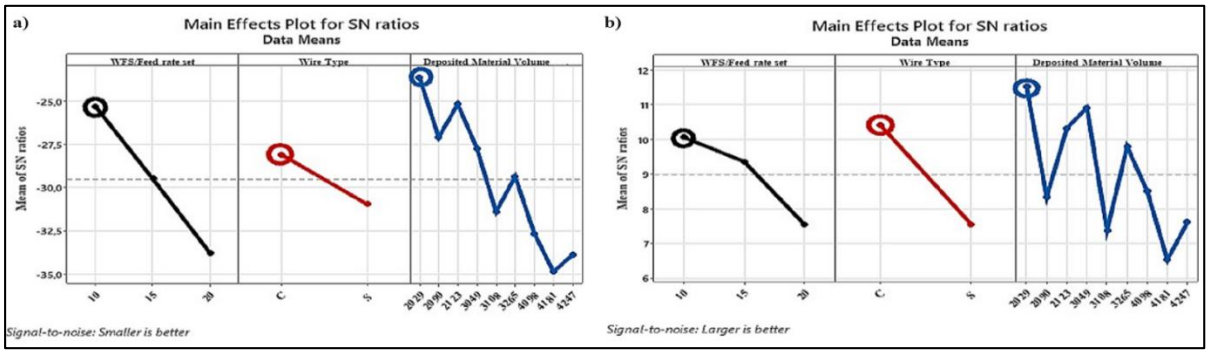

Figure 13. Main affects plots for (a) S/N ratios for t and (b) DR

Table 4. S/N and significance response tables for t (dB) and Dr (dB).

t (dB)				Dr (dB)			
	Wire Type (C or S)	WFS/Feed rate set	Deposited Material Volume (aver.)(mm^3/mm)		Wire Type (C or S)	WFS/Feed rate set	Deposited Material Volume (aver.)(mm^3/mm)
Level	A	B	C	Level	A	B	C
1	-30,97	**-25,30**	**-23,62**	1	7,554	**10,056**	**11,513**
2	**-28,10**	-29,50	-27,09	2	**10,417**	9,356	8,336
3		-33,81	-25,17	3		7,545	10,319
4			-27,73	4			10,908
5			-31,41	5			7,375
6			-29,37	6			9,784
7			-32,66	7			8,503
8			-34,87	8			6,525
9			-33,91	9			7,606
Delta	2,87	8,51	11,25	Delta	2,863	2,511	4,988
Rank	3	2	1	Rank	2	3	1
Output parameter: **Optimum t (sec.):**			**$A_2B_1C_1$**	Output parameter: **Optimum Dr (kg/h):**			**$A_2B_1C_1$**
Analyze method			Taguchi	Analyze method			Taguchi

The most effective parameters affecting the metal deposition rate and deposition time were determined by the Anova module in Minitab software. The examination of the most effective parameters made in the Anova module confirmed that the most effective factor on deposition rate was WFS. The module also confirmed that the WFS/Feed rate set was a direct determinant of welding time, weld bead depth of influence, and heat input. To make the results given in Table 5. more understandable, the S/N values given in bold characters in Table 4. are circled in the graph in Figure 13.

Table 5. Taguchi analyses results and S/N ratios

Exp. no.	Control factors			Total welding time (second)	Deposited rate (kg/h)	S / N ratio for t (dB)	S / N ratio for Dr (dB)
	Wire Type	WFS/Feed rate set	Deposited Material Volume (aver.)(mm^3/mm)				
1	S1	10	2090	32,00	1,85	-30,1030	5,3336
2	S2	10	2123	24,00	2,48	-27,6042	7,9043
3	S3	10	2029	19,20	2,97	-25,6660	9,4414
4	S7	15	3108	48,00	1,80	-33,6248	5,1100
5	S8	15	3265	36,00	2,50	-31,1261	7,9588
6	S9	15	3049	28,80	2,90	-29,1878	9,2480
7	S13	20	4247	64,00	1,92	-36,1236	5,6526
8	S14	20	4181	48,00	2,48	-33,6248	7,8931
9	S15	20	4098	38,40	2,97	-31,6866	9,4451
10	C4	10	2090	16,00	3,69	-24,0824	11,3387
11	C5	10	2123	13,71	4,33	-22,7435	12,7342
12	C6	10	2029	12,00	4,78	-21,5836	13,5850
13	C9	15	3108	28,80	3,03	-29,1878	9,6399
14	C10	15	3265	24,00	3,81	-27,6042	11,6096
15	C11	15	3049	20,57	4,25	-26,2653	12,5688
16	C13	20	4181	64,00	1,81	-36,1236	5,1574
17	C14	20	4098	48,00	2,39	-33,6248	7,5617
18	C15	20	4247	38,40	3,01	-31,6866	9,5589

Table 6. Polynomial regression analyses of two wires's real and predicted equations The results of the wires are given in Table 6. The wires were subjected to independent polynomial regression analyses.

Table 6. Polynomial regression analyses of two wire's real and predicted equations results of H, L, h, DR, HI

Polynomial regression analyses of solid wire real and predicted equations result of H, L, h, DR, HI		
L versus Predicted L	L= - 2,840 + 1,607 Predicted L- 0,03154 Predicted L^2	R^2=93,8 %
H versus Predicted H	H = 2,015 + 0,1719 Predicted H+ 0,07933 Predicted H^2	R^2=93,8 %
h versus Predicted h	h = - 0,426 + 1,460 Predicted h - 0,1162 Predicted h^2	R^2=53,0 %
HI versus Predicted HI	HI = 0,2636 + 0,8669 Predicted HI + 0,01554 HI^2	R^2=99,7 %
DR versus Predicted DR	DR=0,0083+0,9941 Predicted DR+0,00098Predicted DR^2	R^2=99,8 %
Polynomial regression analyses of metal cored wire real and predicted equations result of H, L, h, DR, HI		
L versus Predicted L	L= 5,828 - 0,290 Predicted L + 0,06919 Predicted L^2	R^2=90,73%
H versus Predicted H	H = 9,704 - 3,303 Predicted H + 0,4526 Predicted H^2	R^2 =71,6 %
h versus Predicted h	h = -0,3085+1,374 Predicted h -0,1139 Predicted h^2	R^2=74,88%
HI versus Predicted HI	HI = 0,1135+0,9451 Predicted HI+0,00613 Predicted HI^2	R^2=99,38%
DR versus Predicted DR	DR = 0,0112 + 0,9922 Predicted DR + 0,00120 Predicted DR^2	R^2=99,61%

Note: In the above Table 6 is H (mm): weld bead height, L (mm): weld bead width, h (mm): weld bead depth of influence, HI (kJ/cm): heat input, deposited rate: DR, $p<0.001$.

3.2. Macrostructure Examination Results

Photographs of double-layered macro sections of deposits produced using solid wire and metal-cored wire are given in Figures 11. and 12. In the macrostructure images of the source region of double layer deposits, a burning notch in S18 and a lack of penetration were observed in C6, C12, C18, and S3. In addition, the melting line of the seams, deposited area, area of influence, and heat-affected zone were clearly seen in the macrostructure images. In addition, it was known in previous studies that in multilayer welding processes, the second layer reduces the size of the grains with the normalization effected by applying a kind of heat treatment to the next layer [14–47, 48]. If WFS was increased, the depth of influence and heat input would also increase. All measurements of the bead geometry measured in Table 7. were obtained by scanning and measuring the bead macro section images in the Image J program.

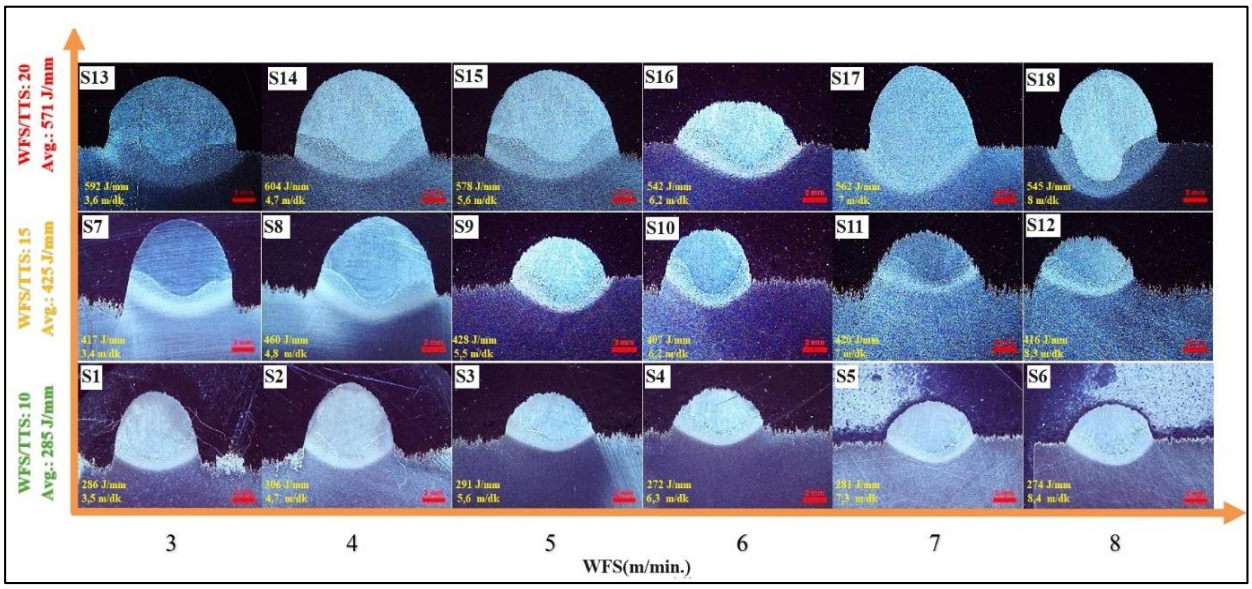

Figure 14. Macrostructure images of solid wire

Deposited material volume values were given in Table 7. according to heat input. They were automatically measured by the metalworm machine. The diameter of the wires was 1.2 mm, and the specific mass of the wires was 7.85 g/cm3. These were entered into the system at the beginning of the experiments. In addition, 1 meter long solid wire: 8.48±0.005 gr and 1 meter long metal cored wire: 8.47±0.005 gr were measured. The difference of 0.01 grams was due to the difference in the production method of both wires. This difference was neglected because it did not create a difference that would affect the results when comparing the wires at the same heat input.

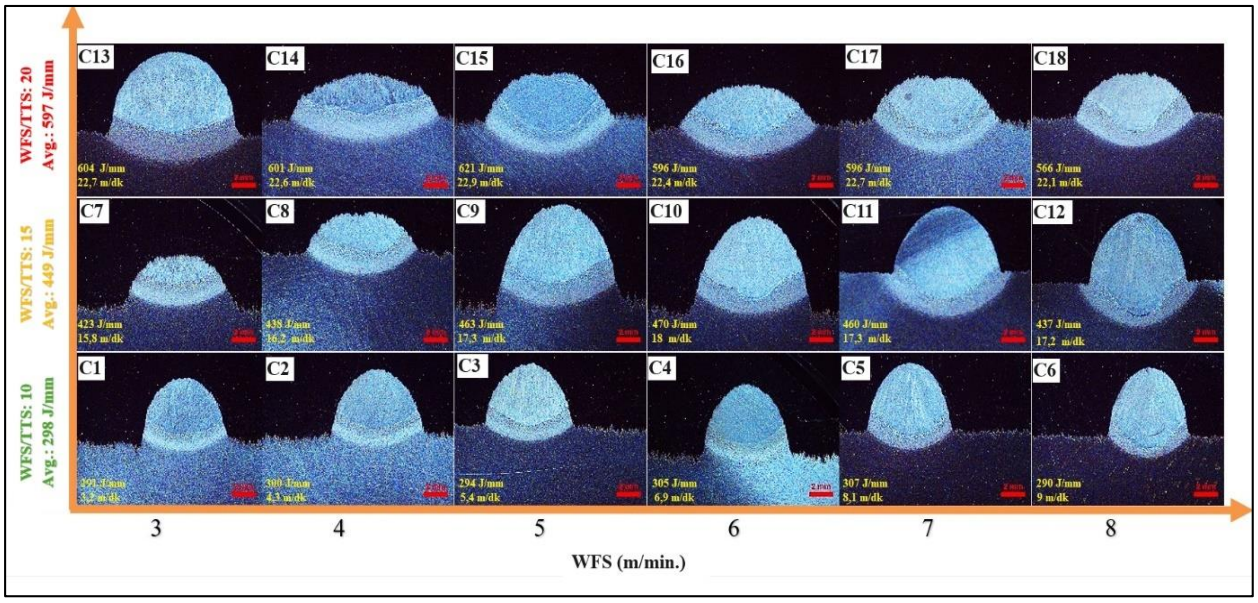

Figure 15. Macrostructure images of solid wire

It can be concluded from Table 7. that in metal-cored wire, as heat input (-) decreased, H, DR (+) increased, and L, h (-) decreased. In solid wire, as the heat input (-) decreased, H (+) increased, and DR, L, and h (-) decreased. This situation was expected from metal-cored wire [7]. Metal-cored wires gave a high deposition rate and high bead height at low heat input [29, 35, 49, 56]. Because to have high strength and high hardness in the phase transformation of this type of high-strength steel, t8/5 (cooling time from 800 ºC to 500 ºC) must be kept low (desired toughness must be reached) [7]. Figure 16. shows the macro-section views of selected samples with the same low heat input. It can be concluded from Figure 16. that metal-cored wire had less production time and a higher deposition rate than solid wire. In the literature, studies conducted with metal-cored wires have shown that metal-cored wires provide a better deposition rate, penetration depth, and uniform penetration profile than solid wire. [2,39,50,51]. Additionally, metal-cored wires provided high-speed material transfer and deeper penetration than solid wires [52].

Table 7. Control parameters, solid/metal-cored wire bead geometry, average hardness values.

Heat Input Intensity	Wire Type	WFS/TTS (torch travel speed) Set	Torch travel speed (m/min)	Deposited Material Volume at 160 mm Seam Length (mm3)	Deposited Rate (kg/h)	Welding Time (second)	Weld Bead Height: H (mm)	Weld Bead Width: L (mm)	Weld Bead Depth of Influence: h (mm)	Area Of Influence (mm2):S1	Deposited Area (mm2):S2
LOW	S1	10	0,30	2090±43	1,85	32,00	5,50	7,60	0,90	5303	28152
	S2	10	0,40	2123±43	2,48	24,00	5,53	8,00	1,19	7118	30897
	S3	10	0,50	2029±43	2,97	19,20	4,90	7,50	1,15	8123	26340
MEDIUM	S7	15	0,20	3108±106	1,80	48,00	4,90	7,30	1,30	6607	31953
	S8	15	0,27	3265±106	2,50	36,00	5,50	7,30	1,45	12760	31907
	S9	15	0,33	3049±106	2,90	28,80	5,80	7,15	1,68	9852	29130
HIGH	S13	20	0,15	4247±115	1,92	64,00	3,00	8,40	0,75	6300	25305
	S14	20	0,20	4181±115	2,48	48,00	3,27	9,42	2,11	12929	23272
	S15	20	0,25	4098±115	2,97	38,40	7,40	10,00	1,75	10492	56890
LOW	C4	10	0,60	2090±43	3,69	16,00	7,92	10,39	0,80	8268	52082
	C5	10	0,70	2123±43	4,33	13,71	5,40	11,00	4,03	29600	35300
	C6	10	0,80	2029±43	4,78	12,00	5,84	8,55	3,61	27730	35791
MEDIUM	C9	15	0,33	3108±106	3,03	28,80	6,82	11,21	2,58	21107	56564
	C10	15	0,40	3265±106	3,81	24,00	3,86	12,70	2,18	20021	34005
	C11	15	0,47	3049±106	4,25	20,57	3,90	10,86	3,19	29483	26469
HIGH	C13	20	0,15	4247±115	1,81	64,00	3,42	11,78	2,61	22139	27511
	C14	20	0,20	4181±115	2,39	48,00	3,50	11,00	2,90	21654	30696
	C15	20	0,25	4098±115	3,01	38,40	3,61	10,02	2,55	19912	24999

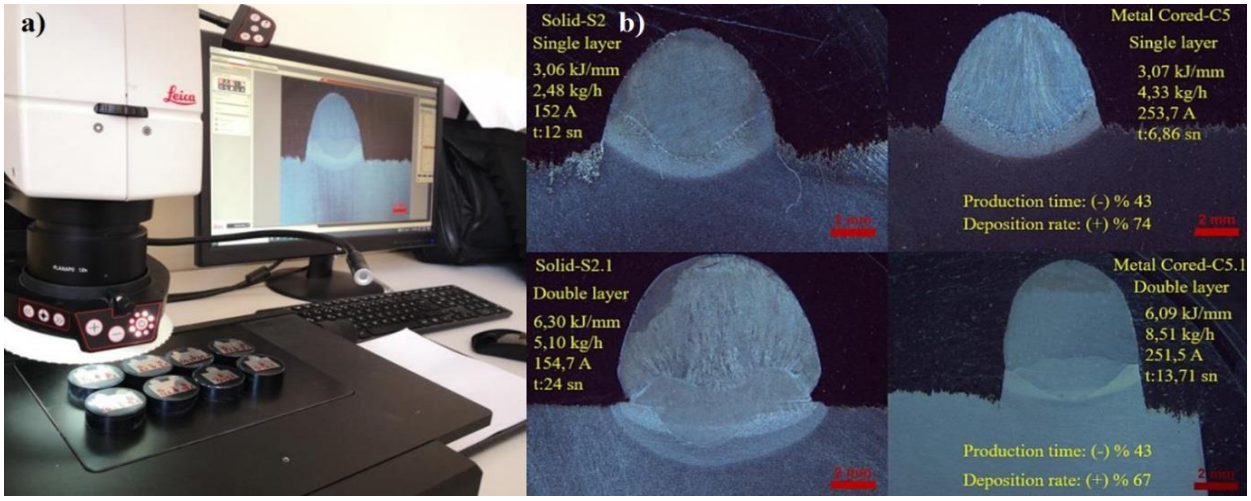

Figure 16. (a) Leica DM 4000M optical microscope at Gazi University, (b) macro section views and compering of result parameters of selected samples with the same low heat input.

3.3. Hardness Test Results

As seen in an example macro section photograph in Figure 10., a total of 20 hardness measurements were made from 7 regions. The average results of these hardness measurements were shown in Table 8, and the detailed results were seen in Figure 18. and Figure 19. Considering the results in Table 8. generally higher hardness was obtained at low heat inputs. It was also known from studies in the literature that hardness values in fine grain structures of high strength and low alloy steels (HSLA) were high [14,47,48]. In materials with fine grain structure, dislocations got stuck in more grain boundary obstacles, which increased the strength and hardness. The Hall-Petch relation was also valid for HSLA steels. It was known that as the carbon equivalence of alloying elements increased in the weld metal region shown in Figure 10., the hardness gradually increased depending on the decrease in the critical cooling rate [53,54]. The hardness gradually increased in parallel with the cooling rate in phases such as fine pearlite, upper bainite, lower bainite and martensite, respectively. In Figure 17.b, high austenitizing temperatures and time enlarged the coarse austenite grains. In coarse austenite grains, there were fewer grain boundaries where a new phase could nucleate. Therefore, the diffusion-controlled transformation mechanism of austenite was delayed, and instead, the transformation to martensite (diffusion-independent transformation) occurred, which was dependent on time and temperature [53, 54]. Coarse-grained martensite could be easily obtained from coarse-grained austenite, but obtaining fine-grained martensite from fine-grained austenite was more preferred in terms of mechanical properties.

In other words, phases containing fine-grained ferrite-cementite emerge as much as there was fine-grained austenite before the transformation [53–55]. In Table 8., Figure 18, and Figure 19, there is no important distinction in mean hardness, maximum hardness, or HAZ hardness at the equal WFS/TTS. However, as the WFS and TTS increased in both wires, the hardness values decreased.

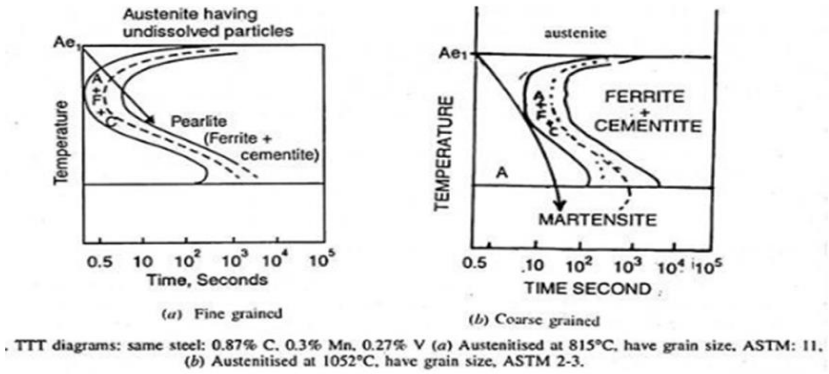

Figure 17. Time-temperature-transformation diagram for the same type of steel (a) Fine-grained austenite ASTM:11 at 815 °C, (b) Coarse-grained austenite ASTM:2-3 at 1052 °C [58]

Table 8. Average hardness values results

Hardness Table (HV1)	Solid Wire			Metal Cored Wire		
	WFS/TTS=10	WFS/TTS=15	WFS/TTS=20	WFS/TTS=10	WFS/TTS=15	WFS/TTS=20
Overall average hardness	308	218	283	304	255	284
Overall maximum hardness	441	278	432	426	378	412
HAZ average hardness	290	217	259	286	229	267

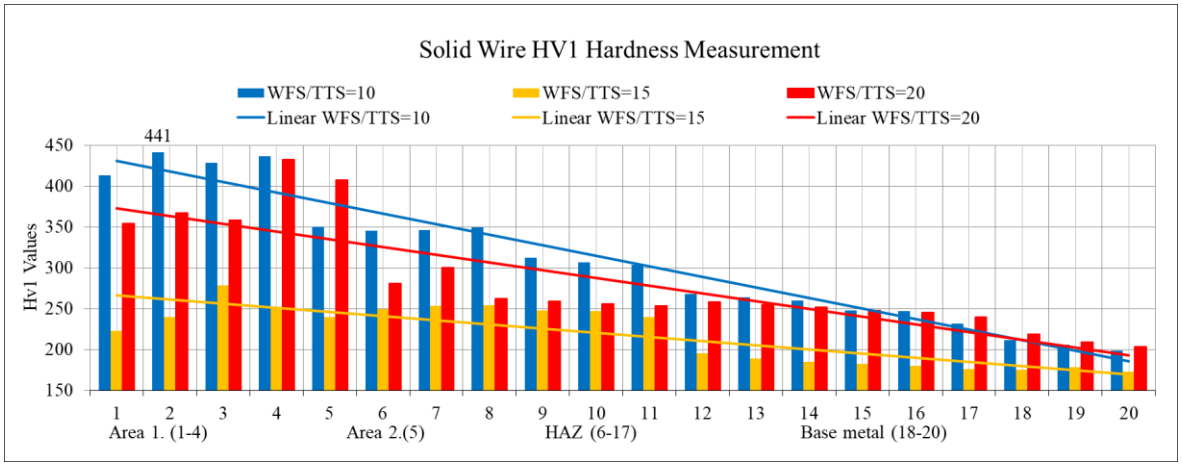

Figure 18. Hardness values measured from macrostructures of solid wire.

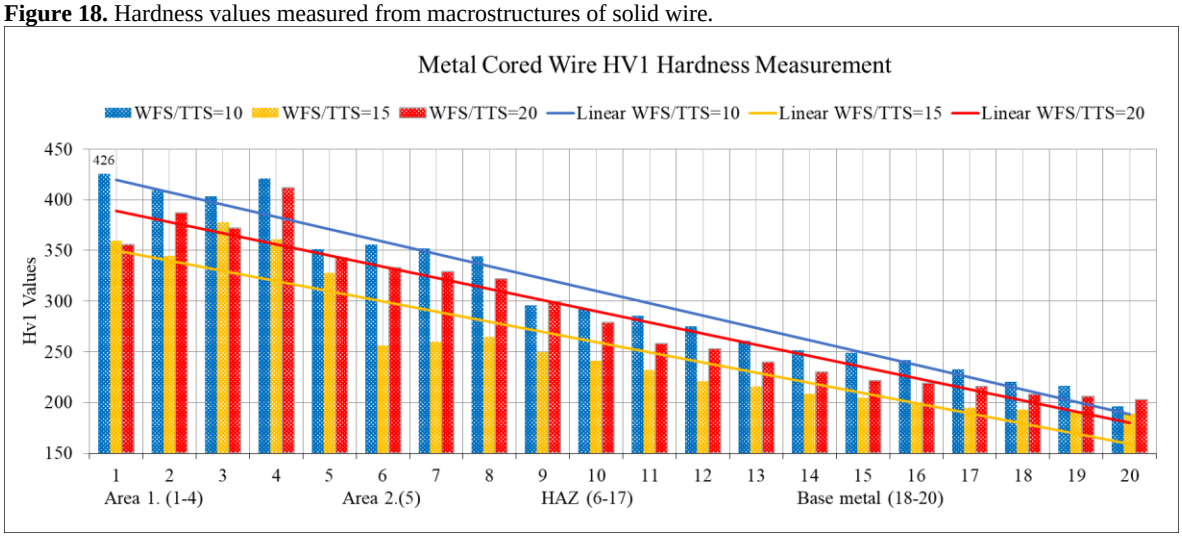

Figure 19. Hardness values measured from macrostructures of metal cored wire.

4. CONCLUSION

In this study, the impacts of control factors (wire type, WFS/feed rate set, deposited material volume) on the result variables (total welding time, deposited rate) were examined both experimentally and through Taguchi analyses. This study confirmed that metal-cored wire had some advantages over solid wire:

- Metal-cored wire not only minimized production time but also maximized metal deposition rate compared to solid wires.
- Metal-cored wire reduced the production time by fifty percent compared to solid wire. It was confirmed that metal-cored wire had a higher deposition rate (1,74 times that of solid wire) and faster melting conditions compared to solid wire at the same heat input.
- In general, as the heat input intensity (WFS/feed rate set) increased in both wires, the hardness decreased linearly.
- On average, the hardness values of cored wire were higher than those of solid wire. This is an important factor for armor steels used in the defense industry. It would make manufacturing possible with fewer layers, in a shorter time, and with the same hardness as the main material.
- Multiple regression analyses showed that deposited rate, total welding time, weld bead depth of influence, and heat input could be estimated without the need to re-experiment with the same wire again. It was good that the real equations and predicted equations results of H, L, h, DR, and HI were compared. The R2 values were between 70% and 95%. This situation confirmed that the experiment results overlapped with the Taguchi analysis results.
- There was a positive linear relationship between heat input (WFS/feed rate set) and weld bead width and depth of influence. However, apart from solid wire, a negative linear relationship was observed between heat input (WFS/feed rate set) and bead height and deposition rate.
- The detection of the most effective parameters in the Anova module, including deposition rate, welding time, and weld bead depth of influence, relied heavily on the WFS.

Also, further experimental investigations are needed to comprehend the ballistic endurance of the wires.

DECLARATION OF ETHICAL STANDARDS

The author(s) of this manuscript declare that the materials and methods used in their studies do not require ethics committee approval and/or special legal permission.

AUTHORS' CONTRIBUTIONS

Mustafa Harman: conceptualization, investigation, methodology, software, and writing (original draft)
Cemil Çetinkaya: supervision, review.
Oğuzhan Yılmaz: supervision, validation, editing.
Nevzat Bol: robotic programming.

ACKNOWLEDGMENT

This study was supported by the Gazi University BAP unit (Project No. FDK-2022-8106). We would also like to thank Intecro Robotics, Automation, R&D, Engineering, and Machinery Industry Trade Incorporated Company, which provided WAAM machine infrastructure support in carrying out this study.

CONFLICT OF INTEREST

There is no conflict of interest in this study.

REFERENCES

[1] Çam, G. "Prospects of producing aluminum parts by wire arc additive manufacturing (WAAM)", ***Materials Today: Proceedings***, 62 (1), 77–85, (2022).
[2] Güler, S., Serindağ, H.T., and Çam, G., "Wire Arc Additive Manufacturing (WAAM): Recent Developments and Prospects," ***Engineer and Machinery***, 63 (706), 82–116 (2022).
[3] Çam, G., and Günen, A. "Challenges and opportunities in the production of magnesium parts by directed energy deposition processes", ***Journal of Magnesium and Alloys***, 12, 1663-1686 (2024).
[4] Wengang Z., Wu N., and Zhou W., "Effect of interpass temperature on wire arc additive manufacturing using high-strength metal-cored wire," **Metals**, 12(212), 1–15, (2022).
[5] Kumar, A.; Maji, K., "Selection of process parameters for near-net shape deposition in wire arc additive manufacturing by genetic algorithm." ***Journal of Materials Engineering and Performance***, 29, 3334–3352 (2020).
[6] Tomaz, I.d.V., Colaço F.H.G., Sarfraz S., Pimenov D.Y., Gupta M.K., and Pintaude G., "Investigations on quality characteristics in gas tungsten arc welding process using an artificial neural network integrated with a genetic algorithm," ***The International Journal of Advanced Manufacturing Technology***, 113, 3569–3583, (2021).
[7] Internet: Fronius International GmbH (Fronius International).Web: https://applications.fronius.com/WeldCubeDemo/RoboticsTool/Start.html. Last access date: June 22, 2024.
[8] L. J. L.Z. et. al., "Review of Wire Arc Additive Manufacturing for 3D Metal Printing," ***Int. J. of Automation Technology***, Vol. 13, No. 3, (2019).
[9] [9] Lee S.H., "Optimization of cold metal transfer-based wire arc additive manufacturing processes using gaussian process regression," ***Metals***, 10, 461, (2020).
[10] Szost, B.A., Terzi, S.; Martina, F., Boisselier, D., Prytuliak, A., Pirling, T., Hofmann, M., Jarvis, D.J., "A comparative study of additive manufacturing techniques: residual stress and microstructural analysis of CLAD and WAAM-printed Ti-6Al-4V components", ***Materials and Design***, 89, 559–567 (2016).
[11] Paskual, A., Álvarez, P., and Suárez, A., "Study on arc welding processes for high deposition rate additive manufacturing", ***Procedia CIRP***, 68, 358–362 (2018).
[12] Zhang, C., Li, Y., Gao, M., and Zeng, X., "Wire arc additive manufacturing of Al-6Mg alloy using variable polarity cold metal transfer arc as power source," ***Materials Science and Engineering***, 711, 415–42 (2018).

[13] Yalçın, M., "Examination of Microstructure and Mechanical Properties of the Welded Regions in Fine-Grained High-Strength Construction Steel," ***Master's Thesis,*** Marmara University Institute of Science and Technology, Istanbul, 1-107 (2008).

[14] Bölükbaşı, Ö.S., Serindağ, T., Gürol, U., A. Günen, A., and Çam, G., "Improving oxidation resistance of wire arc additive manufactured Inconel 625 Ni-based superalloy by pack aluminizing", ***CIRP Journal of Manufacturing Science and Technology***, 46, 89–97, (2023).

[15] Günen A., Gürol U., Koçak M., and Çam G., "Investigation into the influence of boronizing on the wear behavior of additively manufactured Inconel 625 alloy at elevated temperature," ***Progress in Additive Manufacturing***, 8, 1281–1301 (2023).

[16] Günen A., Gürol U., Koçak M., and Çam G., "A new approach to improve some properties of wire arc additively manufactured stainless steel components: simultaneous homogenization and boriding," ***Surface & Coating Technology***, 460, 129395 (2023).

[17] Gürol, U., Altınay, Y., Günen, A., Bölükbaşı, Ö.S., Koçak, M., and Çam, G. "Effect of powder-pack aluminizing on microstructure and oxidation resistance of wire arc additively manufactured stainless steels", ***Surface & Coating Technology***, 468, 129742, (2023).

[18] Ceritbinmez F., Günen A., Gürol U., and Çam G., "A comparative study on the drillability of Inconel 625 alloy fabricated by wire arc additive manufacturing," ***Journal of Manufacturing Processes***, 89, 150–169, (2023).

[19] Internet: Total Materia. The world's most comprehensive material database. Web: https://www.totalmateria.com/page.aspx?ID=Home&LN=TR. Last access date: June 25, 2024.

[20] Küçük Z., "Comparison of Tangential and Orthogonal Turning-Milling Methods Using Taguchi Experimental Design Method," ***Master's Thesis***, Fırat University Institute of Science and Technology, (2017).

[21] Roy R.K., "A primer on the Taguchi Method," Ellen J. Kehoe, ***Society of Manufacturing Engineers***, 2009942461, United States of America (2010).

[22] Nas, E., and Özbek, N.A., "Optimization of the machining parameters in turning of hardened hot work tool steel using cryogenically treated tools," ***World Scientific Publishing Company***, 27: 1–14 (2019).

[23] Kapçak E., "Optimization of welding process parameters using the Taguchi method: an application for nut welding operation," ***Master's Thesis***, Balıkesir University Institute of Science and Technology, (2022).

[24] Callister D.W., Rethwisch D.G., "Materials Science and Engineering (Trans. K.General)", ***Nobel Academic Publishing Education Consultancy Trade Limited Company***, Ankara: 343–390 (2014).

[25] Wen C., Wang Z., Deng X., Wang G., Devesh R., Misra K. "Effect of Heat Input on the Microstructure and Mechanical Properties of Low Alloy Ultra-High Strength Structural Steel Welded Joint", ***Steel research int.***, 89, (2018).

[26] Almeida P., "Innovative process model of Ti–6Al–4V additive layer manufacturing using cold metal transfer (CMT)", ***The 21st annual international solid freeform fabrication symposium***, vol. 2010, University of Texas at Austin (2010).

[27] Cadiou S., Courtois M., Carin M., Berckmans W., and Le Masson P., "3D heat transfer, fluid flow, and electromagnetic model for cold metal transfer wire arc additive manufacturing (Cmt-Waam)", ***Additive Manufacturing***, 36, 101541, (2020).

[28] Ayarkwa K.F., Williams S., and Ding J., "Investigation of pulse advance cold metal transfer on aluminum wire arc additive manufacturing," ***International journal of rapid manufacturing,*** 5 (1), 44–57 (2015).

[29] Trinh, N.Q., Tashiro, S., Suga, T., Kakizaki, T., Yamazaki, K., Lersvanichkool, A., Bui, H.V., and Tanaka, M. "Metal transfer behavior of metal-cored arc welding in pure argon shielding gas," ***Metals***, 12, 1577 (2022).

[30] XU X., "Wire + Arc Additive Manufacture of New nd Multiple Materials," ***Doctoral Thesis***, Cranfield University School of Aerospace, Transport, and Manufacturing (2017).

[31] Kara, S., and Korkut, M.H., "Investigation of the Effect of Heat Treated After Welding on Strength of Joints in Used Armored Combat Vehicles," ***Journal of Defense Sciences***, 11 (2), 159–171 (2012).

[32] Tülbentçi, K., "MIG-MAG Gas Welding Method". ***Arctech Welding Electrodes Publication***, Publication No. 2, İstanbul, 1-55. (1998).

[33] Güner M., "Examining the effect of electrode type (bare wire or flux-cored wire) on weld bead properties in MAG welding," ***Master's Thesis***, Yıldız Technical University, Institute of Science and Technology, (2007).

[34] Işık A.O., "Examining the Effect of Electrode Type on Weld Seam Properties in MAG Welding," ***Master's Thesis***, Yıldız Technical University Institute of Science and Technology, (2014).

[35] Sanyal S., Chandra S., Kumar S., and Roy G.G., "An Improved Model of Cored Wire Injection in Steel Melts," ***ISIJ International***, 44, 1157–1166, (2004).

[36] Özkan, E., "Characterization of the Submerged Arc Welding Flux and Flux Cored Wire Combination, Which Fulfills The Required Mechanical and Metallurgical Properties, For Industrial Applications," ***Doctoral Thesis***, Ege University Institute of Science and Technology, (2015).

[37] Adonyi, Y., "HAZ Properties in High-Performance Steel Solid-State Welds," ***CWA Conference***, 1-20, Longview (2014).

[38] Internet: TWI Training & Examination Services EWF/IIW Diploma Course Presentation Web: https://slideplayer.com/slide/1568314/.Last access date: 03.04.2024.

[39] Vora J., Parikh N., Chaudhari R., Patel V.K., Paramar H., Pimenov D.Y., and Giasin K., "Optimization of Bead Morphology for GMAW-Based Wire-Arc Additive Manufacturing of 2.25 Cr-1.0 Mo Steel Using Metal-Cored Wires," ***Applied Sciences***, 12, 5060. (2022).

[40] Chaudhari R., Parikh N., Khanna S., Vora J., and Patel V., "Effect of multi-walled structure on microstructure and mechanical properties of 1.25Cr-1.0Mo steel fabricated by GMAW-based WAAM using metal-cored wire," ***Journal of Material Research and Technology***, 21: 3386–3396, (2022).

[41] Internet: BÖHLER X 90-IG Solid wire, low-alloyed, high strength. https://rebels-grup.ro/wp-content/uploads/2020/10/Bohler_X90-IG.pdf. Last access date: June 22, 2024.

[42] Internet: BÖHLER alform® 900 MC metal-cored wire. https://www.voestalpine.com/welding/uk-en/company/news-and-events/welding-consumables-

for-crane-and-lifting/ . Last access date: (2024).
[43] Internet: Manufacture process of seamless cored wire: Voestalpine Böhler Welding https://www.youtube.com/watch?v=4CdbXF_T5ss. Last access date: June 22, 2024.
[44] Akkurt, A., "Waterjet Cutting Systems and Assessment of Their Industrial Applications," ***Journal of Polytechnic***, 7(2), 129–139 (2004).
[45] Harman M., Ada H., and Çetinkaya C., "Introduction of Weldability of High Strength Steels Using Different Welding Methods," ***Master's Thesis***, Gazi University Graduate School of Natural and Applied Sciences (2019).
[46] Ada, H., "Optimisation Of The Welding Parameters Of Joints Of Api Pipes With Taguchi Method," ***Doctoral Thesis***, Gazi University Institute of Science and Technology, Ankara, (2017).
[47] Bhadeshıa, H. K. D. H. Bainite in steels transformations, microstructure, and properties. London: ***Cambridge University Pess***, (2001).
[48] Lin Z., Goulas C., Ya W., and Hermans M.J.M., "Microstructure and mechanical properties of medium carbon steel deposits obtained via wire and arc additive manufacturing using metal-cored wire metals," ***Metals***, 9, 673 (2019).
[49] Gürol U., Dilibal S., Turgut B., and Koçak M., "Characterization of a low-alloy steel component produced with a wire arc additive manufacturing process using metal-cored wire," ***Materials Testing***, 64(6): 755–767, (2022).
[50] Harati, E., Jose, B., & Igestrand, M., "Wire arc additive manufacturing using high-strength steel tubular and solid wires," ***Welding International***, 38(5), 329–334, (2024).
[51] Pixner F., Buzolin R., Zelic A., Riedlsperger F., Orlowska M., Warchomicka F., Decherf M., Lasnik M., and Enzinger N., "Tailoring the alloy composition for wire arc additive manufacturing utilizing metal-cored wires in the cold metal transfer process," ***Materials & Design***, 215, 110453, (2022).
[52] Tümer M., Vallant R., Warchomicka F.G.,, Enzinger N. "Undermatched Welding of Ultra-High-Strength Steel S1100 with Metal-Cored Wire: Influence of Welding Positions on Mechanical Properties", ***Journal of Materials Engineering and Performance***, 31:7068–7079, (2022).
[53] Callister D., Rethwisch W. G., "Translation From The 8th Edition Of Materials Science And Engineering," ***Nobel Academic Publishing Education Consultancy Trading Limited Company***, Ankara, 343–390 (2014).
[54] Kang B.Y., Kim H.J., and Hwang S.K., "Effect of Mn and Ni on the Variation of the Microstructure and Mechanical Properties of Low-carbon Weld Metals," ***ISIJ International***, 40 (12), 1237–1245 (2000).
[55] Zhang Z., Farrar R.A., "Influence of Mn and Ni on the Microstructure and Toughness of C-Mn-Ni Weld Metals," ***Welding Research Supplement***, 183–196 (1997).
[56] Harman M., Ada H., and Çetinkaya C., "Determination of the effect of filler metal type on metallurgical and mechanical properties in welding of QStE420TM steel by MAG welding method," ***Journal of Polytechnic***, 23(2), 321-332 (2020).
[57] Harman M., Ada H., and Çetinkaya C. "Investigation of QStE420TM steel material weldability using different basic electrodes by electric arc welding method," ***Journal of the Faculty of Engineering and Architecture of Gazi University***, 37(4), 2041–2056, (2022).
[58] J.G. Silva, F., Santos, J., and Gouveia, R., "Dissolution of Grain Boundary Carbides by the Effect of Solution Annealing Heat Treatment and Aging Treatment on Heat-Resistant Cast Steel," Hk30. ***Metals***, 7 (251), 1–12 (2017).
[59] Ríos, S., Colegrove, P.A., Williams, S.W., "Metal transfer modes in plasma Wire+ Arc additive manufacture," ***Journal of Materials Processing Technology***, 264, 45–54 (2019).